Electronic Supplementary Material (ESI) for Nanoscale Advances.

Ultra-broadband Near-Perfect Metamaterial Absorber for Photovoltaic Application: Electronic Supplementary Information

1. MATERIAL PROPERTIES

The complex refractive index, $\tilde{n}$ of a material is described by,

$$\tilde{n} = \mathrm{n} + i\kappa. \tag{S1}$$

Here, n and κ are the real part and imaginary part of the complex refractive index. The n determines the speed of the light in the medium, and the κ is responsible for scattering and absorption which is also called the extinction coefficient. The (n, κ) data of $Al_xGa_{1-x}As$ (x = 0.3), Ge, GaAs, and Ti are presented in Fig. S1.

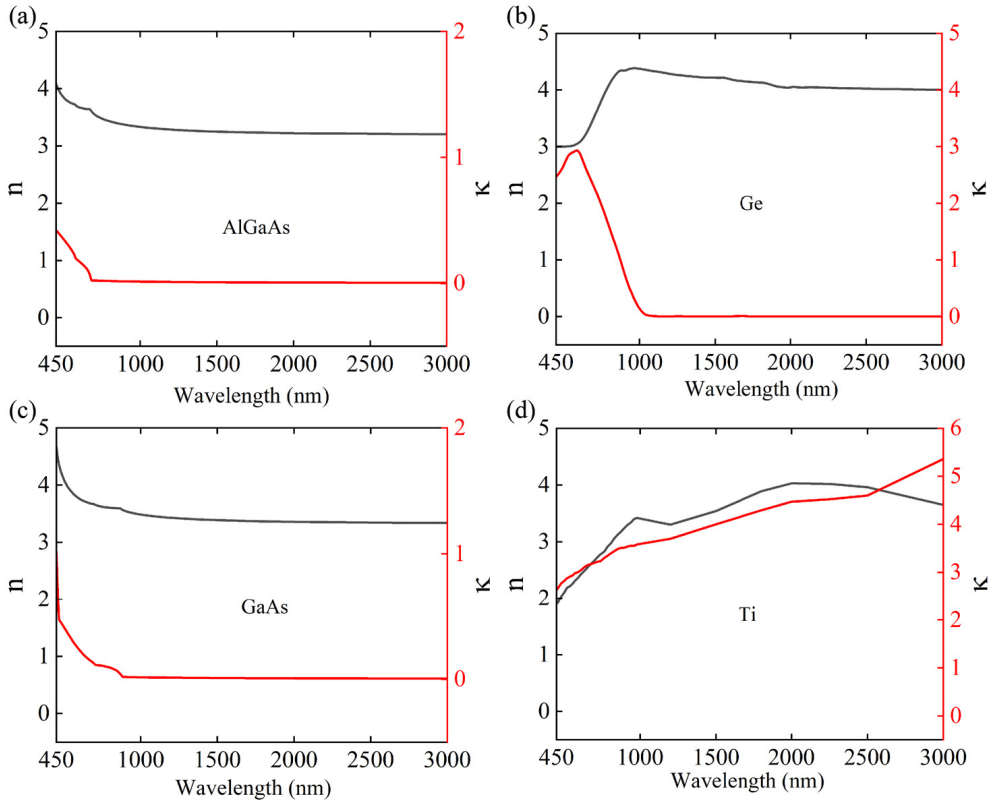

Fig. S1. Refractive index (n) and extinction coefficient (κ) spectra of (a) $Al_xGa_{1-x}As$ (x = 0.3) [1], (b) Ge, (c) GaAs, and (d) Ti [2].

Table S1. Utilized materials parameters in heat transfer equation

Parameters	Unit	AlGaAs	Ge	GaAs	Ti
Density	Kg m^{-3}	2329	5327	5320	4510
Specific heat	J kg^{-1} K^{-1}	366	360	322	522.3
Thermal conductivity	$Wm^{-1}K^{-1}$	3.3	60	46	11.4

Table S2. Utilized materials parameters in the SCAPS-1D simulation tool

Parameters	Unit	AlGaAs	Ge	GaAs
Bandgap	eV	1.58 (direct)	0.7 (indirect)	1.42 (direct)
Thickness	nm	60	120	30
Electron affinity	eV	3.74	4.00	4.07
Donor density	cm^{-3}	1.0×10^{6}	2.4×10^{13}	1.0×10^{16}
Acceptor density	cm^{-3}	1.0×10^{16}	2.4×10^{13}	1.0×10^{6}
CB effective density of states	cm^{-3}	6.5×10^{17}	1.0×10^{19}	3.95×10^{17}
VB effective density of states	cm^{-3}	1.1×10^{19}	5.0×10^{18}	9.1×10^{18}
Electron thermal velocity	cms^{-1}	3.77×10^{7}	3.1×10^{7}	4.4×10^{7}
Hole thermal velocity	cms^{-1}	1.65×10^{7}	1.9×10^{7}	1.8×10^{7}
Electron mobility	$cm^2V^{-1}s^{-1}$	2300	3900	8500
Hole mobility	$cm^2V^{-1}s^{-1}$	145.6	1800	470
Dielectric permittivity	–	12.04	16	12.9

2. SOLVER PHYSICS

The finite-difference time-domain (FDTD) method can obtain frequency solutions using Fourier transforms. Consequently, a comprehensive array of valuable parameters can be computed, including the complex Poynting vector and light's transmission and reflection characteristics. Fields are calculated by,

$$\frac{\partial \overrightarrow{D}}{\partial t} = \nabla \times \overrightarrow{H}, \tag{S2}$$

$$\overrightarrow{D}(\omega) = \epsilon_0 \epsilon_r(\omega)\, \overrightarrow{E}(\omega), \tag{S3}$$

$$\frac{\partial \overrightarrow{H}}{\partial t} = -\frac{1}{\mu_0} \nabla \times \overrightarrow{E}, \text{ and} \tag{S4}$$

$$\epsilon_r(\omega) = n^2. \tag{S5}$$

Here, $\overrightarrow{D}$, $\overrightarrow{H}$, and $\overrightarrow{E}$ denote the displacement, magnetic, and electric fields, respectively. ϵ_0 and ϵ_r represent the dielectric constants at vacuum and medium where n is the complex refractive index. For two-dimensional FDTD simulation, we had four fields, such as $\overrightarrow{E_x}$, $\overrightarrow{E_z}$, $\overrightarrow{H_x}$, and $\overrightarrow{H_z}$, to calculate transmission, reflection, and absorption.

3. ABSORPTION SPECTRA COMPARISON OF DIFFERENT STRUCTURES

The question of "why double grating?" is answered here. The absorption drastically dropped for wavelengths longer than 1500 nm without the Ti back reflector layer. The absorption increased for longer wavelengths when the Ti back reflector layer was added, as depicted in Fig. S2. Therefore, the Ti layer is essential for absorbing longer wavelengths. The single grating structure in Fig. S2 (black line) shows a lower absorption in visible wavelength with a moderate absorption in

the medium wavelength range, and declining absorption was observed at longer wavelengths. AlGaAs slab-topped structure (red line) exhibited better absorption in higher wavelengths with a dip around 500 nm; however, the peak of the solar irradiance spectra is at 500 nm. The GaAs layer was employed as an absorption enhancer. The structure without the GaAs layer demonstrated a declination in absorption spectra, increasing reflection across the whole wavelength range, as seen in Fig. S2 (blue line). Carriers may be recombined and lost in the interface states of Ti – GaAs surface. Back surface recombination can be reduced by introducing a higher band gap material layer to create a barrier between the absorber and the metal layer. A high band gap oxide layer of 4 eV was utilized, as depicted in Fig. S2(e) [3].

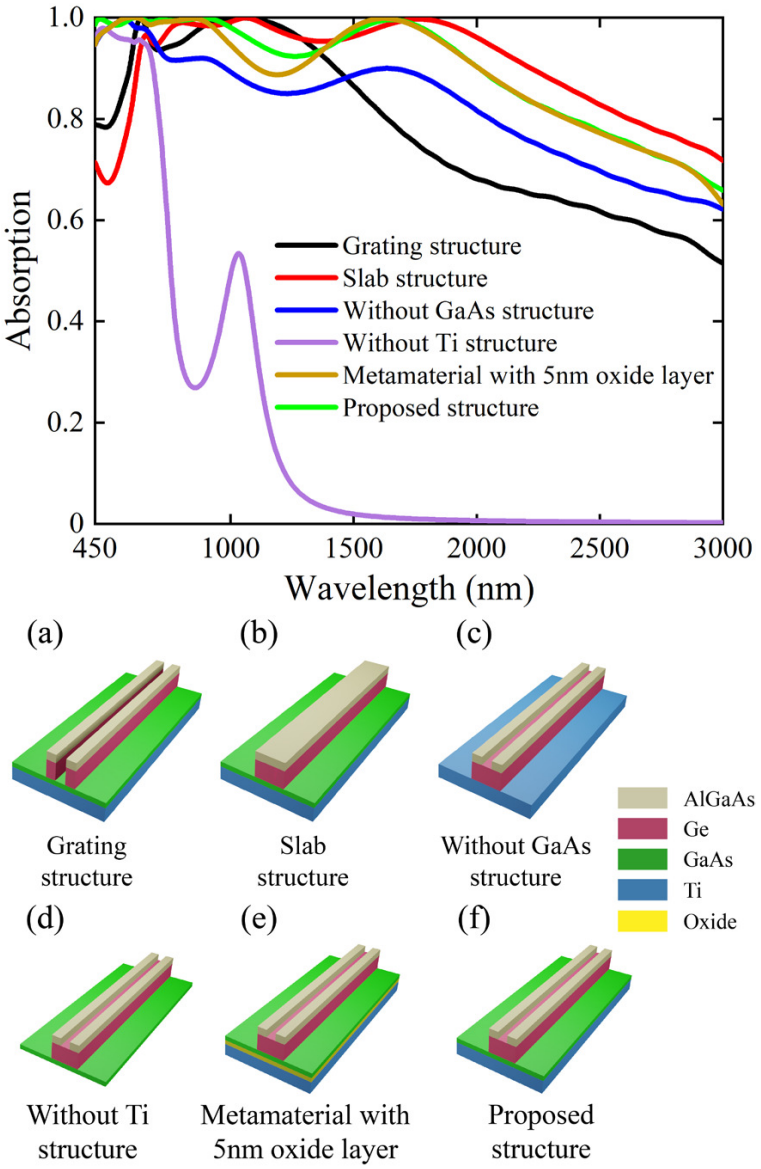

Fig. S2. The effect of different structures (a) grating, (b) slab, (c) without GaAs, (d) without Ti, (e) with 5 nm oxide layer, and (f) our proposed structures on absorption spectra under TM-polarized light.

4. BAND GAP ESTIMATION USING TAUC PLOT EXTRAPOLATION

The band gap indicates the threshold excitation energy at which photons can be absorbed. We calculated the estimated band gap of our proposed double-grating metamaterial structure by

using [4],

$$\alpha h\nu = A(h\nu - E_g)^n. \tag{S6}$$

Here, α, $h\nu$, and A denote the absorption coefficient, energy, and constant. The bandgap of the proposed structure under TM-polarized incident light was calculated to be 0.5 eV, as shown in Fig. S3(a). Similarly, Figs. S3(b) and (c) exhibited the approximated band gaps of 1.02 eV and 0.93 eV for TE-polarized and unpolarized light, respectively. We can relate bandgap in terms of absorption. The proposed structure exhibited maximum absorption due to a lower effective band gap under TM-polarized light. Conversely, the bandgap was highest for TE-polarized incident light because of the directional characteristics of the structure.

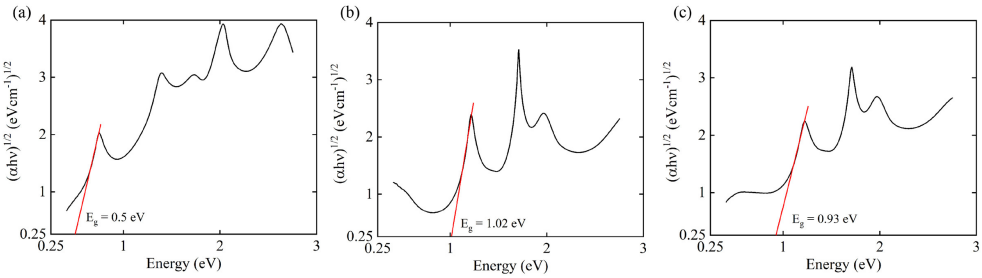

Fig. S3. The Tauc plot of our proposed double grating metamaterial structure under (a) TM polarized, (b) TE polarized, and (c) unpolarized incident light. Here, the tangential line of the first peak provides the bandgap of the structure. The structure exhibited lower band gap under TM-polarized light than that of TE-polarized light.

5. ABSORPTION, REFLECTANCE AND TRANSMITTANCE SPECTRA FOR UNPOLARIZED LIGHT

Our proposed double grating structure exhibited an average absorption of 87% for unpolarized incident light as can be seen in Fig. S4. For a majority of the wavelength regime, the absorption was above 80%. The amount of light transmitted is negligible as depicted in Fig. S4.

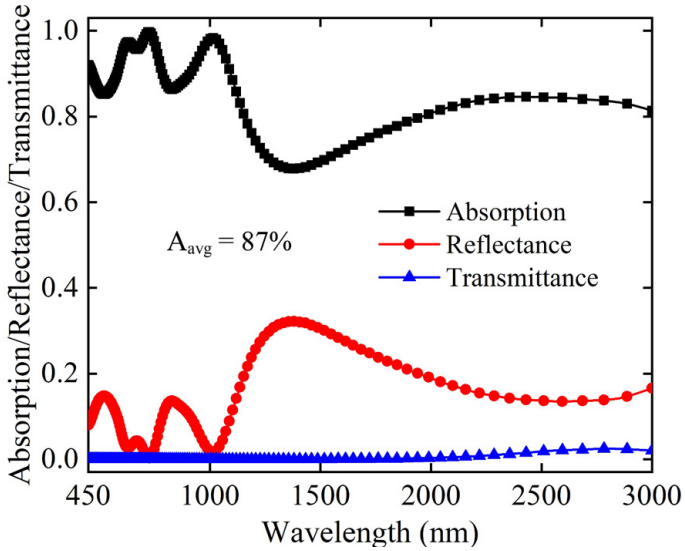

Fig. S4. Absorption, reflectance, and transmittance spectra of the metamaterial absorber for unpolarized incident light.

6. ABSORBED AND UNUSED ENERGY SPECTRA

Fig. S5 shows the absorbed and unused energy spectra under AM 1.5 G solar irradiance light. The absorbed and unused energy of the proposed structure was obtained to be 96.5% and 3.5%

under TM-polarized incident light as seen in Fig. S5(a). The unused energy of TE-polarized light increased due to the directional nature of the structure. The structure under unpolarized light had similar absorbed energy spectra to TM-polarized incident light as shown in Fig. S5(c). Thus, we can infer that the proposed structure has a high absorption efficiency across the entire wavelength range (450 nm – 3000 nm).

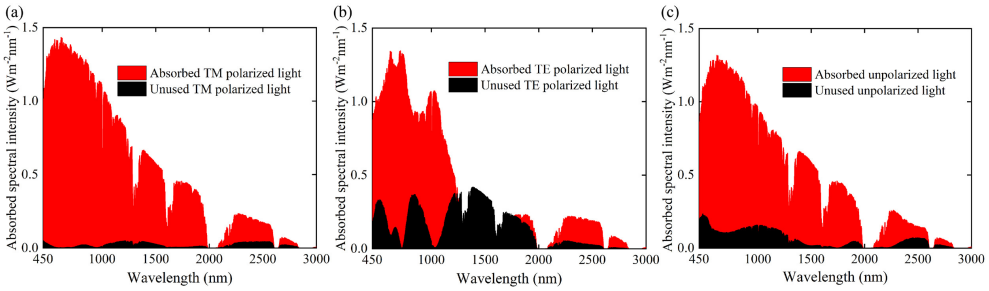

Fig. S5. Absorbed and unused energy spectra of the double grating proposed metamaterial structure under AM 1.5 G solar irradiance for (a) TM-polarized incident light, (b) TE-polarized incident light, and (c) Unpolarized incident light.

7. EFFECTS OF INCIDENCE ANGLE ON ABSORPTION SPECTRA

Fig. S6 represents the color plot of calculated absorption spectra for different incidence angles of TM, TE, and unpolarized lights. The absorption decreased with the increase in the incidence angle of TM polarized light, as shown in Fig. S6(a). Contrarily, absorption increased when we increased the incidence angle of TE-polarized light, as depicted in Fig. S6(b). We achieved high absorption between 30° and 65° for our proposed structure. The proposed structure exhibited a dip around 500 nm under TE polarized incident light. The absorber structure maintained a constant high absorption beyond 80% for different incidence angles of unpolarized light, as depicted in Fig. S6(c).

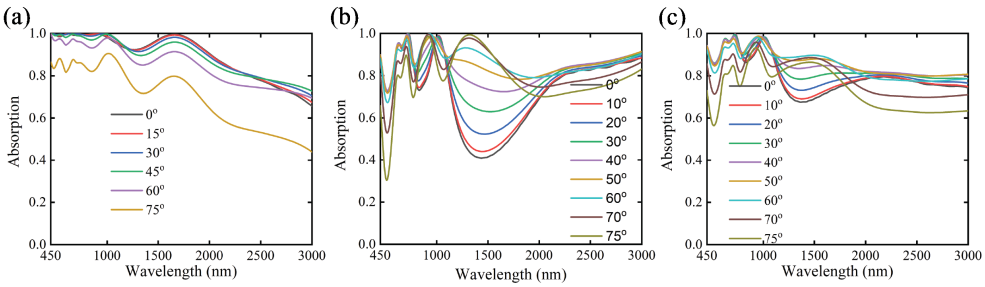

Fig. S6. The line plots of absorption spectra for different incident angles under (a) TM, (b) TE, and (c) unpolarized incident lights.

8. CURRENT DENSITY – VOLTAGE CHARACTERISTICS CURVE FOR STRUCTURES I – IV

As the bandgap of Ge is small compared to structure IV, V_{OC} will be reduced, which results in degraded efficiency, as depicted in Fig. S7(a). Moreover, the bandgap of Ge is far away from the optimum bandgap. Therefore, we obtained a small PCE of 3.87% for the Ge double-grating structure. On the other hand, the bandgap of GaAs is close to the optimum bandgap; however, we achieved a reduced PCE for structure III compared to structure IV due to the homojunction device. Similarly, structures I and II were homojunction-type solar cells; therefore, these structures exhibited reduced PCE and low maximum power density compared to structure IV, as depicted in Fig. S7(b). The solar performance parameters, such as V_{OC}, J_{SC}, FF, and PCE, are enlisted in Table S3. We obtained an excellent PCE of 31.7% for our proposed structure IV, where V_{OC} and J_{SC} were found to be 0.837 V and 47.10 mA/cm2, respectively. Structure IV achieved the maximum power of 31.70 mW/cm2, which is substantially quite high compared to other structures.

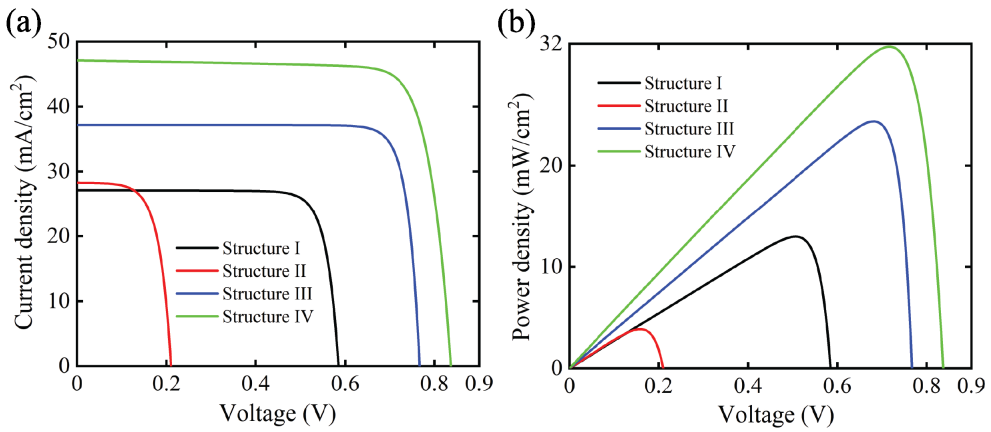

Fig. S7. (a) $J-V$ and (b) $P-V$ characteristics curves of designed four structures under AM 1.5 G solar spectrum.

Table S3. Comparative solar performance analysis of structures I – IV for AM 1.5 G

Structures	V_{OC} (V)	J_{SC} (mA/cm^2)	FF (%)	PCE (%)
Structure I	0.585	27.11	81.83	12.89
Structure II	0.210	28.26	65.15	3.87
Structure III	0.767	37.17	85.40	24.36
Structure IV	0.837	47.10	80.42	31.70

9. EFFECTS OF DOPING ON CURRENT DENSITY-VOLTAGE CHARACTERISTICS CURVE

Fig. S8 depicts the effects of the doping concentration of AlGaAs and GaAs on the $J-V$ characteristics curve. Increasing doping concentrations increases J_{SC}, however reduces V_{OC}. A table of solar performance analysis with varying doping concentrations is enlisted in Table S4.

Table S4. Comparative solar performance analysis of the effects of doping on structure IV

Doping Concentrations (cm^{-3})	V_{OC} (V)	J_{SC} (mA/cm^2)	FF (%)	PCE (%)
10^{13}	0.8475	46.86	78.66	31.24
10^{14}	0.8464	46.93	79.41	31.54
10^{15}	0.8418	47.00	80.00	31.66
10^{16}	0.8370	47.10	80.42	31.70
10^{17}	0.8272	47.43	80.62	31.64

We considered the doping concentrations of 10^{16} cm^{-3} in our numerical calculations.

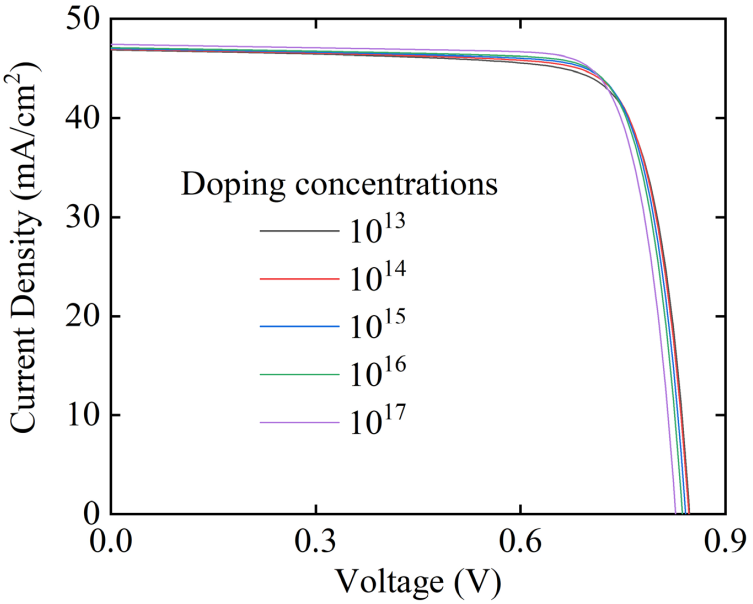

Fig. S8. Effects of doping concentrations on $J - V$ characteristics curve.

10. PERFORMANCE ANALYSIS UNDER TM-POLARIZED LIGHT

Comparative performance analysis of short-circuit current density, J_{SCmax} and light absorption efficiency, LAE for structures I – IV under TM polarized incident light are enlisted in Table S5. J_{SC} and LAE were enumerated by solving the manuscript's Eqs. 5 and 17. The maximum LAEs were calculated to be 99.1% and 96.2% in the wavelength range of 450 – 1000 nm and 450 – 3000 nm for structure IV, respectively, which were higher than those of unpolarized incident light. The theoretically obtained maximum limit of J_{SCmax} under TM-polarized incident light was to be 81.5 mA/cm^2 for our proposed structure.

Table S5. Theoretical limit of maximum J_{SC} and LAE of structures I – IV under TM-polarized light

	J_{SCmax} (mA/cm^2)	LAE (%)	
Structure	300 – λ_g nm	450 – 1000 nm	450 – 3000 nm
Structure I	46.0	98.3	95.5
Structure II	80.1	94.2	95.9
Structure III	53.9	98.0	95.6
Structure IV	81.5	99.1	96.2

11. IMPACT OF AMBIENT TEMPERATURES ON HEAT TEMPERATURE PROFILE

Fig. S9 illustrates the effect of ambient temperatures on the heat temperature profile for our proposed structure. We achieved ∼23° of temperature inclination from its ambient temperature under various ambient temperatures because the absorption of our proposed structure is independent of surrounding temperatures.

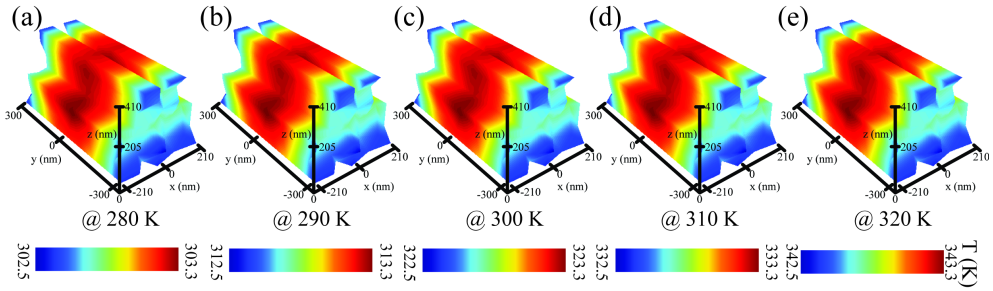

Fig. S9. Evolution of heat temperature profiles of the proposed metamaterial double-grating structure under different ambient temperatures including (a) 280 K, (b) 290 K, (c) 300 K, (d) 310 K, and (e) 320 K.

REFERENCES

1. S. Adachi, "Optical dispersion relations for gap, gaas, gasb, inp, inas, insb, alxga1-x as, and in1-xgaxasyp1-y," J. Appl. Phys. **66**, 6030–6040 (1989).
2. E. D. Palik, "Front matter," in *Handbook of Optical Constants of Solids*, E. D. PALIK, ed. (Academic Press, Boston, 1998), p. iii.
3. V. M. Mikoushkin, V. V. Bryzgalov, S. Y. Nikonov, A. P. Solonitsyna, and D. E. Marchenko, "Composition and band structure of the native oxide nanolayer on the ion beam treated surface of the gaas wafer," Semiconductors **52**, 593–596 (2018).
4. A. Hassanien and A. A. Akl, "Effect of se addition on optical and electrical properties of chalcogenide cdsse thin films," Superlattices Microstruct. **89**, 153–169 (2016).